Sixth International Symposium on Turbulence and Shear Flow Phenomena
Seoul, Korea, 22-24 June 2009

INVESTIGATION OF THE BOUNDARY LAYERS IN TURBULENT RAYLEIGH-BÉNARD CONVECTION

Matthias Kaczorowski
Institute of Aerodynamics and Flow Technology
German Aerospace Center (DLR)
Bunsenstr. 10, D–37073 Göttingen, Germany
matthias.kaczorowski@dlr.de

Anna Ebert
Dept. of Mechanical Engineering
Technical University of Ilmenau
P.O. 100565, D–98684 Ilmenau, Germany

Claus Wagner
Institute of Aerodynamics and Flow Technology
German Aerospace Center (DLR)
Bunsenstr. 10, D-37073 Göttingen, Germany
claus.wagner@dlr.de

André Thess
Dept. of Mechanical Engineering
Technical University of Ilmenau
P.O. 100565, D–98684 Ilmenau, Germany
andre.thess@tu-ilmenau.de

ABSTRACT

In the present study the temperature profiles of turbulent Rayleigh-Bénard convection obtained through DNS and microthermistor measurements in a rectangular container are compared. It is found that both DNS and experimental data are in good agreement when comparing temperature profiles at topologically similar flow positions. It is observed that the data sets obtained at $\mathcal{R}a \approx 10^8$ are in significantly better agreement than at $\mathcal{R}a \approx 10^7$. Finally, our results are compared to the analytical fit function proposed by Shishkina & Thess (2009) and find that this function gives a very good representation of the DNS data when the temperature profiles through the centre of the roll structures are evaluated.

INTRODUCTION

The accurate prediction of the heat transfer between a turbulently moving fluid and a solid wall is despite its importance to engineering applications still a numerically challenging task. Reynolds Averaged Navier-Stokes (RANS) simulations which are typically performed to solve engineering problems suffer from the inherent problem that they have to model all turbulent quantities, whereas Direct Numerical Simulations (DNS) are not normally applicable to complex geometries and highly turbulent flows. In order to be able to improve the modelling of the turbulent quantities it is essential to gain a deeper understanding of the underlying phenomena, where the turbulent boundary layers and their interaction with the bulk flow play a crucial role. Experimental investigations on the other hand have to cope with with problems of accessibility and (simultaneous) data acquisition at different locations.

In fundamentel research the geometrically simple Rayleigh-Bénard experiment is often chosen to investigate the turbulent heat exchange between a thermally driven fluid and a hot bottom and a cold top wall, respectively. The characteristic parameter of this natural convection phenomenon is the Rayleigh number $\mathcal{R}a = \hat{\alpha}\hat{g}\hat{H}^3\Delta\hat{T}/(\hat{\nu}\hat{\kappa})$, which is a non-dimensional measure of the buoyancy and diffusive forces acting on the fluid. Here $\hat{\alpha}$, $\hat{\nu}$ and $\hat{\kappa}$ denote the thermal expansion coefficient, kinematic viscosity and thermal diffusivity, respectively. $\Delta\hat{T}$ is the vertical temperature gradient between the two bounding surfaces, $\hat{H}$ the height of the fluid layer and $\hat{g}$ the gravitational acceleration; $\hat{}$ indicates dimensional quantities.

Hölling & Herwig (2006) theoretically derived a scaling for the temperature profile in turbulent Rayleigh-Bénard convection (RBC) with infinite aspect ratio $\Gamma = \hat{W}/\hat{H}$, and hence no mean flow, in the limit of $\mathcal{R}a \to \infty$. They found a linear scaling of the temperature near the wall (the conductive sublayer) and a logarithmic one well outside the mean boundary layer thickness δ_θ. The shape of the boundary layer at various aspect ratios and Rayleigh numbers was investigated experimentally by du Puits *et al.* (2007) along the axis of a cylindrical cell showing that the boundary layers' shape hardly changes with the cell's aspect ratio. Maystrenko *et al.* (2007) studied the structure of the thermal boundary layers of turbulent RBC in a long rectangular cell. They found significant changes of the structure of the thermal boundary layer in the longitudinal direction which they concluded to be a result of the mean wind. Ebert *et al.* (2008) observed a buffer layer with a power-law behaviour in their Rayleigh-Bénard cell of finite aspect ratio. This led to a separation of the temperature profile into three regions: linear for $x_3^+ \lesssim 0.2$, power law for $0.2 \lesssim x_3^+ \lesssim 3$ and logarithmic for $x_3^+ \gtrsim 8$, where x_3^+ is the wall distance normalised as follows from (4).

In the following we compare the structure of the thermal boundary layer at different locations of a rectangular cell obtained through DNS from the onset of turbulence at $\mathcal{R}a = 3.5 \times 10^5$ until a fully developed turbulent thermal field is achieved at $\mathcal{R}a = 2.31 \times 10^8$. The DNS data is compared to experimental results by Maystrenko *et al.* (2007) and Ebert *et al.* (2008), as well as to an approximation function proposed by Shishkina & Thess (2009), who theoretically analysed the mean temperature profiles of RBC and compared their results to the temporally and spatially averaged profiles obtained through DNS of RBC in a cylindrical container ($\Gamma = 1$) filled with water.

NUMERICAL PROCEDURE

In the present numerical simulations the non-dimensionalisation of the governing equations is carried out using $x_i = \hat{x}_i/\hat{W}$, $u_i = \hat{u}_i/(\hat{\alpha}\hat{g}\Delta\hat{T}\hat{H})^{1/2}$, $\theta = (\hat{T} - \hat{T}_0)/\Delta\hat{T}$, $p = \hat{p}/(\hat{\rho}\hat{\alpha}\hat{g}\hat{H}\Delta\hat{T})$ and $t = \hat{t}(\hat{\alpha}\hat{g}\Delta\hat{T}\hat{H})^{1/2}/\hat{W}$. Together with the Boussinesq approximation one obtains the

Table 1: Simulation parameters of the DNS of turbulent RBC in the rectangular enclosure. N_1, N_2 and N_3 denote the number of grid points in the span wise, longitudinal and vertical direction, $t_{avg.}$ the time over which the statistics are averaged and $\mathcal{N}u|_{top,bottom}$ the Nusselt number averaged over $t_{avg.}$ as well as the top and bottom plates.

$\mathcal{R}a$	N_1	N_2	N_3	$t_{avg.}$	$\mathcal{N}u\|_{top,bottom}$
3.5×10^5	64	320	64	75	6.17 ± 0.04
3.5×10^6	160	576	160	34	12.16 ± 0.10
3.5×10^7	160	576	160	95	22.86 ± 0.08
2.31×10^8	256	800	256	33	39.75 ± 0.35

incompressible Navier-Stokes equations given by (1) - (3)

$$\frac{\partial u_i}{\partial x_i} = 0 \quad (1)$$

$$\frac{\partial u_i}{\partial t} + u_j \frac{\partial u_i}{\partial x_j} + \frac{\partial p}{\partial x_i} = \frac{\mathcal{P}r}{(\Gamma^3 \mathcal{R}a)^{1/2}} \frac{\partial^2 u_i}{\partial x_j^2} + \theta \delta_{3i} \quad (2)$$

$$\frac{\partial \theta}{\partial t} + u_i \frac{\partial \theta}{\partial x_i} = \frac{1}{(\Gamma^3 \mathcal{R}a \mathcal{P}r)^{1/2}} \frac{\partial^2 \theta}{\partial x_i^2}, \quad (3)$$

where u_i are the velocity components in $i = 1, 2, 3$ direction, p and θ are the pressure and temperature, respectively. The simulations are conducted in a rectangular container with aspect ratios $\Gamma_{13} = \hat{W}/\hat{H} = 1$ and $\Gamma_{23} = \hat{L}/\hat{H} = 5$. The lateral walls are adiabatic and top and bottom walls isothermal with non-dimensional temperatures $\theta_{bottom} = +0.5$ and $\theta_{top} = -0.5$, respectively. No-slip and impermeability conditions are applied to all walls and the grid spacing is gradually refined towards the rigid walls, so that the computational domain is discretised using non-equidistant meshes in all three coordinate directions. The volume balance procedure by Schumann *et al.* (1979) is used for the integration over the fluid cells and the solution is evolved in time by means of the explicit Euler-Leapfrog scheme. Spatial derivatives and cell face velocities are approximated by piece-wise integrated fourth order accurate polynomials, where the velocity components are stored on staggered grids as described in detail by Shishkina & Wagner (2007). The velocity pressure coupling is carried out through the projection method by Chorin (1968) which requires the solution of a Poisson equation. Here, a direct solver is employed using a cyclic reduction algorithm. The system of equations is decoupled using the separation of variables method described in Kaczorowski *et al.* (2008).

RESULTS

Global flow structure

In figure 1 isosurfaces of the temperature field illustrate the turbulent RBC in a long rectangular enclosure with solid walls in all coordinate directions for Rayleigh numbers between $\mathcal{R}a = 3.5 \times 10^5$ and $\mathcal{R}a = 2.31 \times 10^8$. The illustration highlights how the large scale plumes forming the large scale circulation disintegrate into smaller plumes that are clustered in regions of rising or falling (not shown) fluid. The two highest Rayleigh numbers of the DNS are close to two cases investigated experimentally by Maystrenko *et al.* (2007) and Ebert *et al.* (2008). It is observed that the flow fields obtained through the DNS reflect four counter rotating convection rolls, whereas two rolls were observed

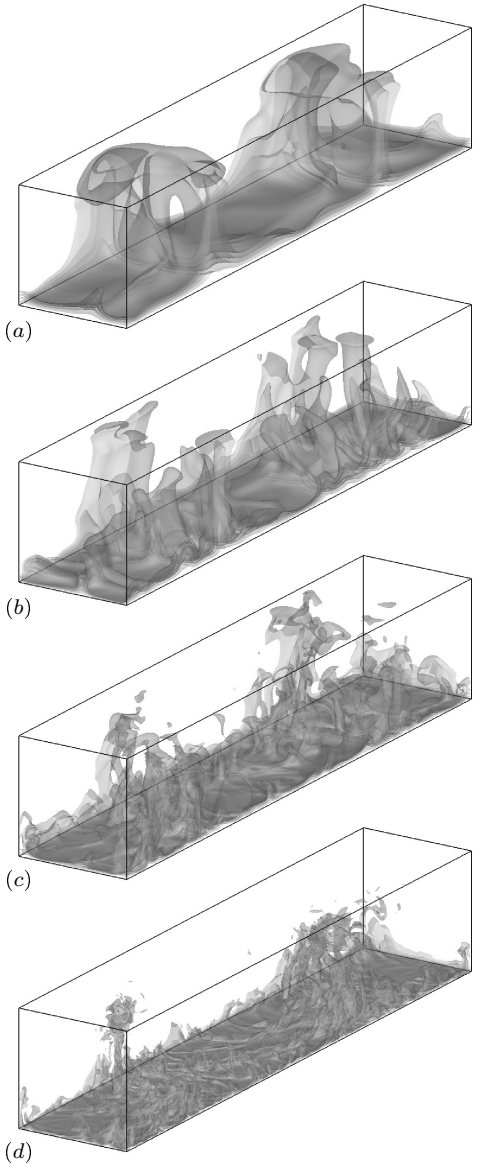

Figure 1: Isosurfaces of temperature for the hot fluid ($\theta \geq 0.1$) and Rayleigh numbers (*a*) $\mathcal{R}a = 3.5 \times 10^5$, (*b*) 3.5×10^6, (*c*) 3.5×10^7 and (*d*) 2.31×10^8.

in the experiment by Maystrenko *et al.* (2007). A four-roll-structure was also found for $\mathcal{R}a \approx 10^8$ by means of LES in the same geometry conducted by Sergent & Le Quéré (2008), whereas they found a two-roll-structure for $\mathcal{R}a \approx 10^{10}$, and for $\mathcal{R}a \approx 10^8$ when the Rayleigh number was approached from a higher $\mathcal{R}a$ with two rolls.

The four-roll-structure of the DNS is also reflected by the variation of the thermal boundary layer thickness in longitudinal (x_2-) direction. This is illustrated in figure 2 in terms of the local Nusselt number $\mathcal{N}u_{loc} = 1/(2\delta_\theta)$, where δ_θ denotes the boundary layer thickness obtained through the maximum rms-value criterion (Belmonte *et al.* , 1994).

Because of the global flow structure the temporally averaged temperature profiles in the centre plane ($x_1 = 0.5$) depend on their longitudinal (x_2) position, which is illustrated for $\mathcal{R}a = 3.5 \times 10^7$ in figure 3. This implies that a mean wind is formed in the rectangular convection cell,

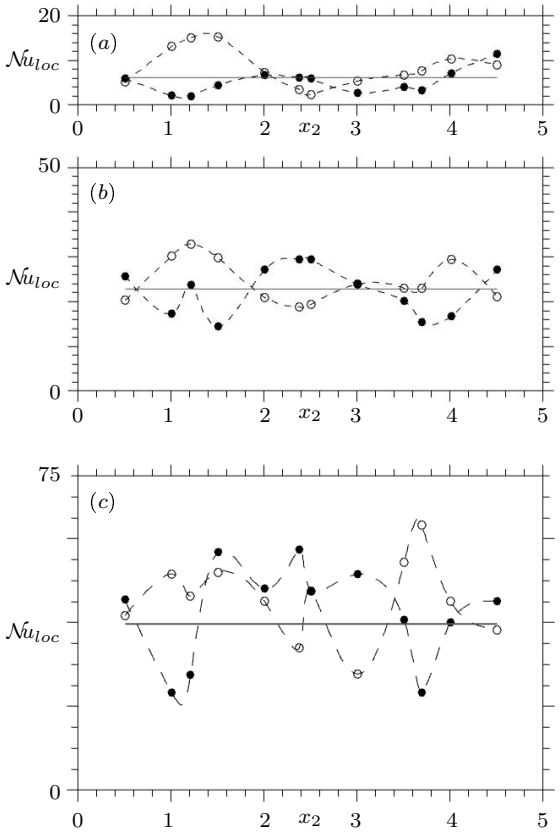

Figure 2: Local Nusselt number $\mathcal{N}u_{loc} = 1/(2\delta_\theta)$ in the centre plane ($x_1 = 0.5$) for (a) $\mathcal{R}a = 3.5 \times 10^5$ and (b) $\mathcal{R}a = 3.5 \times 10^7$ in the hot ($\bullet$) and cold ($\circ$) boundary layer. The solid line indicates the global mean Nusselt number averaged over both horizontal surfaces.

so that in regions with predominantly rising or falling fluid the centre of the cell has temperatures $\theta_c > 0$ or $\theta_c < 0$, respectively. This behaviour is also reflected by the experimentally measured temperature profiles near the top and bottom plates by Maystrenko *et al.* (2007), where the mean temperature does not always match the arithmetic mean temperature of heating and cooling plates. Maystrenko *et al.* (2007) as well consider this to be an effect of the large-scale flow structures. At $\mathcal{R}a = 2.31 \times 10^8$ the numerically obtained temperature profiles show a significantly reduced dependency on the x_2-position, which reflects a more homogeneous mixing for this case.

Analysis of the mean temperature profiles

In order to compare the DNS data with the experimental results both are normalised as

$$x_3^+ = 2\mathcal{N}u_{loc}\,|(x_3 - x_{3,wall})| \quad (4)$$

$$\text{and } \theta^+ = 1 - 2|\theta|, \quad (5)$$

where the horizontal hot or cold walls with a temperature of $\theta^+ = 0$ are located at $x_3^+ = 0$ and $x_3^+ = 1$ represents the edge of the thermal boundary layer at that location. The arithmetic mean temperature of the fluid is then $\theta^+ = 1$. The temperature profiles measured by Ebert *et al.* (2008) in their periferical position ($x_2 \approx 1.20$) for $\mathcal{R}a = 6.0 \times 10^7$ are plotted in figure 4 together with the DNS data for $\mathcal{R}a = 3.5 \times 10^7$. In figure 5 experimental data for $\mathcal{R}a = 6.0 \times 10^8$

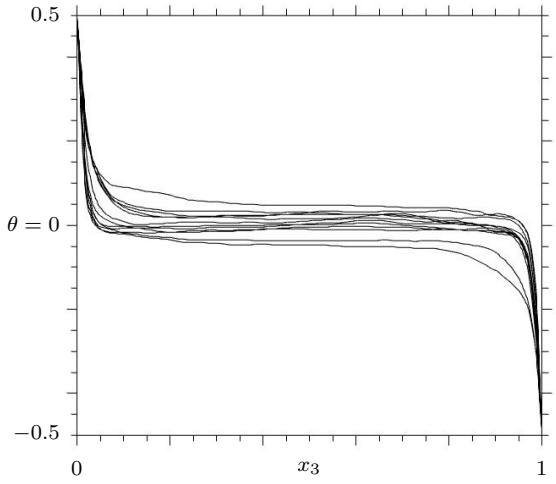

Figure 3: Temporally averaged temperature profiles in the centre plane ($x_1 = 0.5$) at various longitudinal positions for $\mathcal{R}a = 3.5 \times 10^7$.

is compared to DNS data at $\mathcal{R}a = 2.31 \times 10^8$. It is observed that especially for the lower $\mathcal{R}a$ comparison there are clear discrepancies between the DNS and the experimental data that cannot be related to the small difference in Rayleigh number. Especially the cold wall temperature profiles differ significantly. It is obvious that the experimentally measured temperature profiles are significantly more symmetrical than those obtained through the DNS which is believed to be a result of the different global flow structres. Better agreement for the higher $\mathcal{R}a$ case is probably due to the fact that the large-scale structures vanish with increasing $\mathcal{R}a$.

In order to investigate the theoretically predicted and experimentally measured temperature profiles and to analyse whether the profile follows a power-law (6) or an exponential scaling (7), the diagnostic functions

$$\mathcal{P} = \frac{\partial(\ln\theta^+)}{\partial(\ln x_3^+)} \quad (6)$$

$$\text{and } \mathcal{E} = \frac{\partial\theta^+}{\partial(\ln x_3^+)} \quad (7)$$

can be used. It has to be pointed out that the temperature profiles at the higher $\mathcal{R}a$ are in significantly better agreement, especially in the near-wall region, where the DNS predict a lower gradient than the experimentally measured profiles suggest. It follows from figure 4 (b) that the power-law diagnostic function falls below the DNS data for $x_3^+ \lesssim 1$. the higher $\mathcal{R}a$ case data plotted in figure 5, however, is found to be in very good agreement. The exponential diagnostic functions plotted in figure 4 (c) and 5 (c) on the other hand reveal significant differences for $x_3^+ \gtrsim 1$, where the DNS data show a slower decrease of $\mathcal{E}$ for $x_3^+ > 1$.

In figures 6 and 7 experimental and numerical profiles are not compared at the same longitudinal position but for positions through the centre of a roll structure. for this case experimental and numerical data are found to be in excellent agreement as far as the power-law diagnostic function is concerned. A non-negligible offset is found for the exponential diagnostic function. However, the qualitative behaviour is found to be identical.

Self-similar temperature profiles

In figures 4 to 7 we also compare our results to the ap-

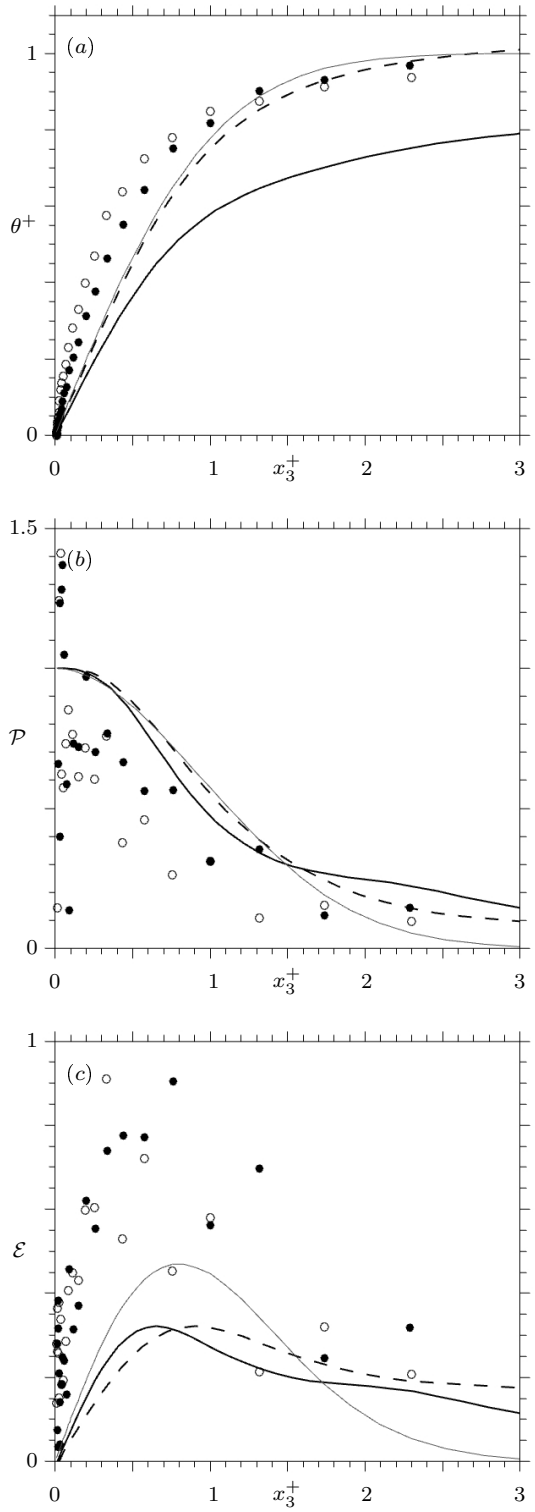

Figure 4: Analysis of the temporally averaged thermal boundary layers (BL) at the position $x_2 \approx 1.20$ and $x_1 = 0.5$: (a) temperature profile, (b) power-law and (c) exponential diagnostic function. DNS data (cold BL: – –, hot BL: —) for $\mathcal{R}a = 3.5 \times 10^7$ is compared to experimental data (cold BL: ○, hot BL: •) for $\mathcal{R}a = 6 \times 10^7$ and the analytical function $\theta^+ \approx 1 - \exp(-x_3^+ - 0.5(x_3^+)^2)$.

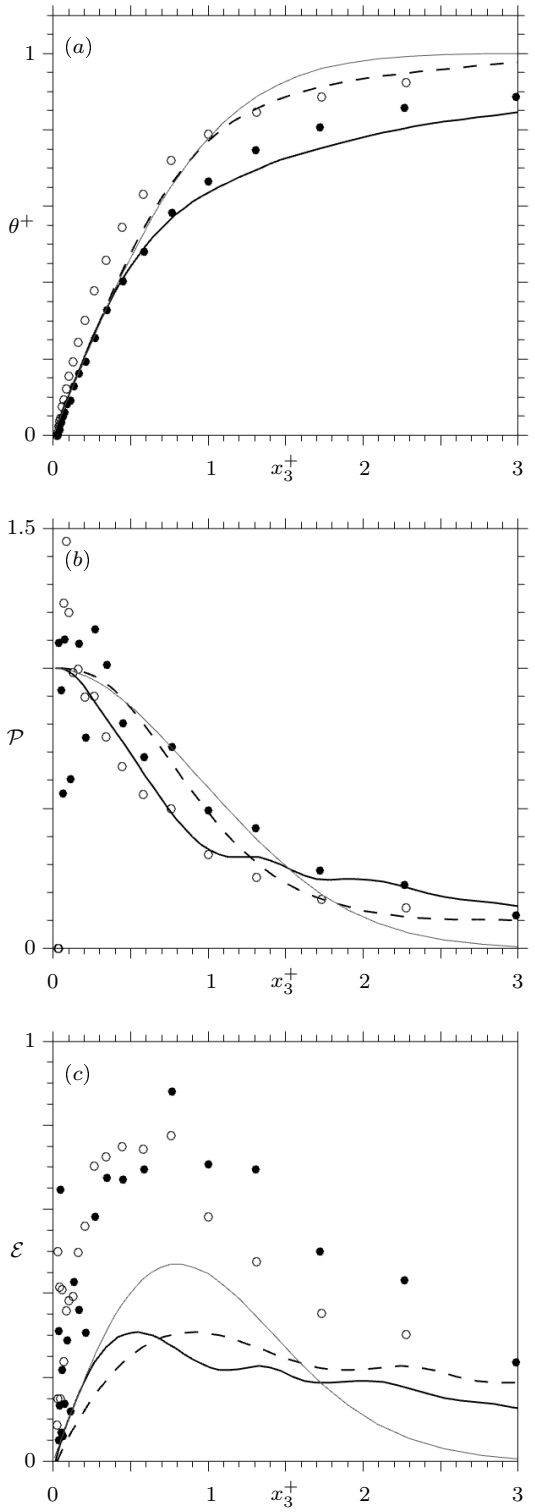

Figure 5: Analysis of the temporally averaged thermal boundary layers (BL) at the position $x_2 \approx 1.20$ and $x_1 = 0.5$: (a) temperature profile, (b) power-law and (c) exponential diagnostic function. DNS data (cold BL: – –, hot BL: —) for $\mathcal{R}a = 2.31 \times 10^8$ is compared to experimental data (cold BL: ○, hot BL: •) for $\mathcal{R}a = 6 \times 10^8$ and the analytical function $\theta^+ \approx 1 - \exp(-x_3^+ - 0.5(x_3^+)^2)$.

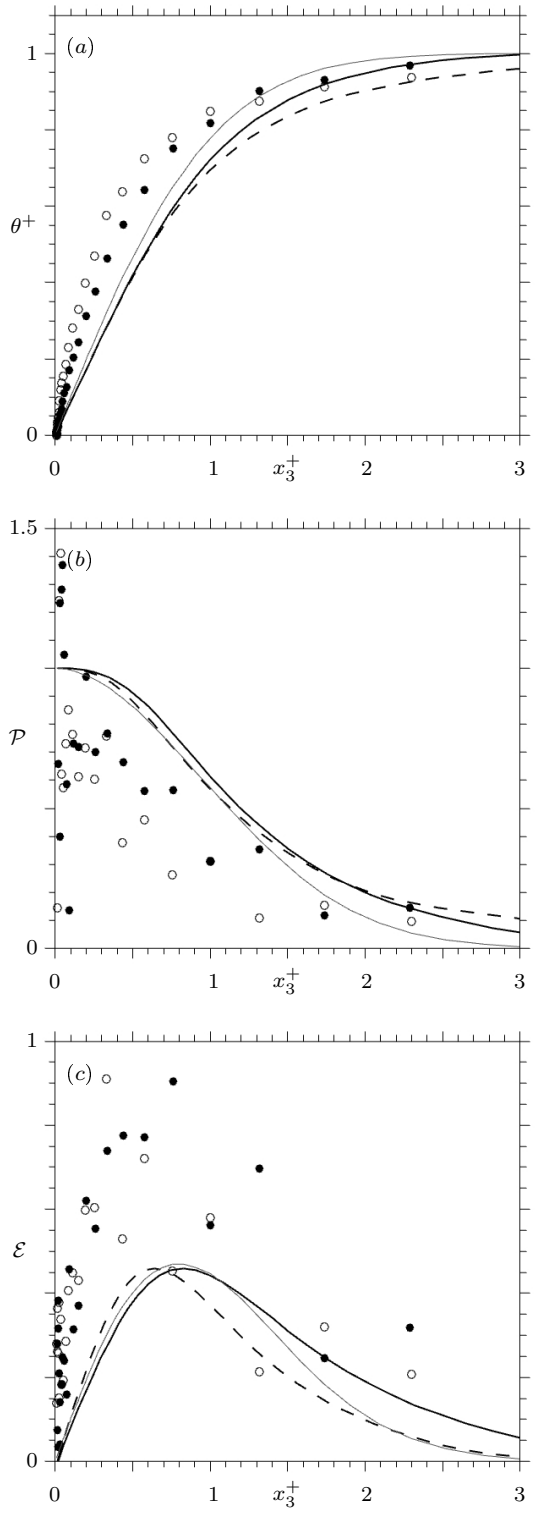

Figure 6: Analysis of the temporally averaged thermal boundary layers (BL) at the position $x_2 \approx 2.00$ and $x_1 = 0.5$: (a) temperature profile, (b) power-law and (c) exponential diagnostic function. DNS data (cold BL: – –, hot BL: —) for $\mathcal{R}a = 3.5 \times 10^7$ is compared to experimental data (cold BL: ○, hot BL: ●) for $\mathcal{R}a = 6 \times 10^7$ and the analytical function $\theta^+ \approx 1 - \exp(-x_3^+ - 0.5(x_3^+)^2)$.

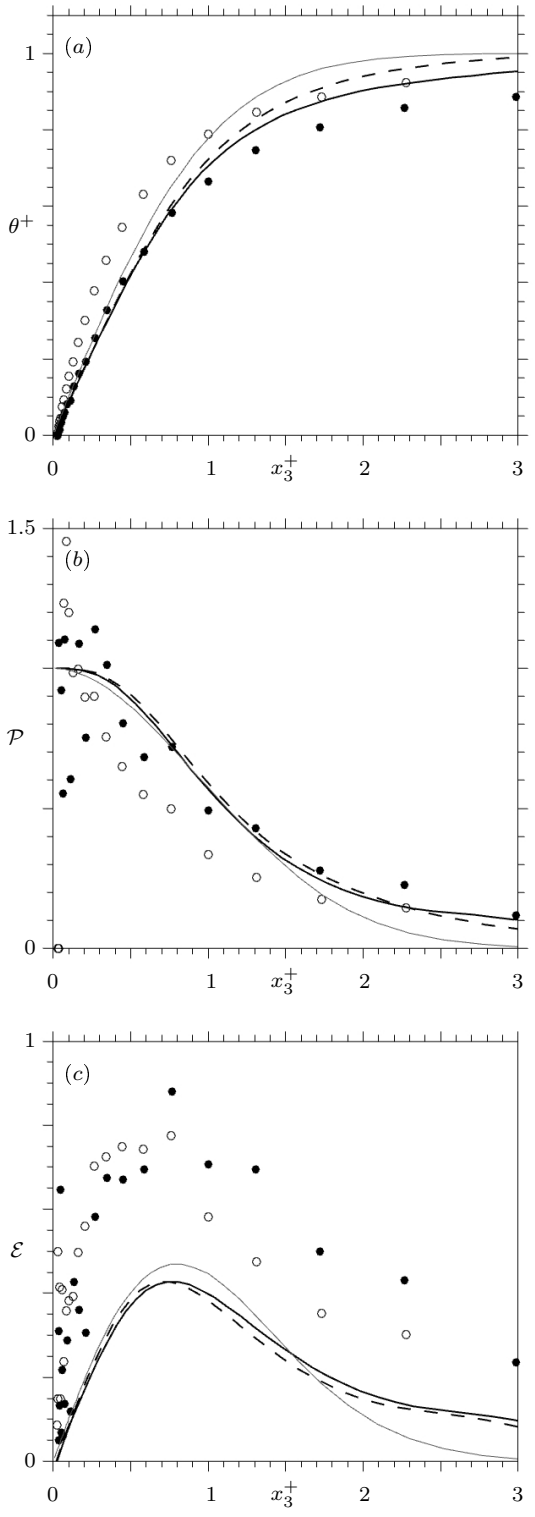

Figure 7: Analysis of the temporally averaged thermal boundary layers (BL) at the position $x_2 \approx 2.00$ and $x_1 = 0.5$: (a) temperature profile, (b) power-law and (c) exponential diagnostic function. DNS data (cold BL: – –, hot BL: —) for $\mathcal{R}a = 2.31 \times 10^8$ is compared to experimental data (cold BL: ○, hot BL: ●) for $\mathcal{R}a = 6 \times 10^8$ and the analytical function $\theta^+ \approx 1 - \exp(-x_3^+ - 0.5(x_3^+)^2)$.

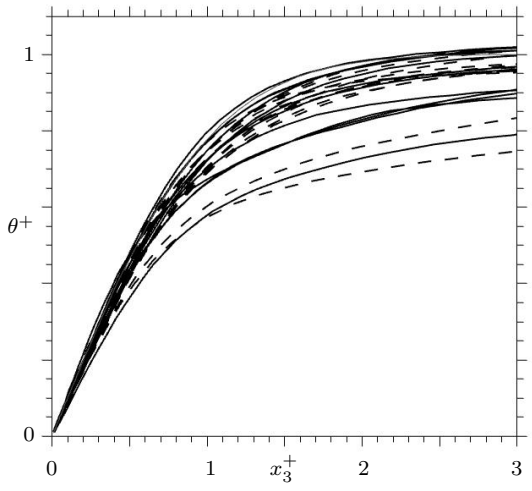

Figure 8: Normalised temperature profiles of the DNS at $\mathcal{R}a = 3.5 \times 10^7$ plotted in inner coordinates for 12 longitudinal positions in the centre plane $x_1 = 0.5$ (cold BL: – –, hot BL: —).

proximation function

$$\theta^+ \approx 1 - \exp(-x_3^+ - 0.5(x_3^+)^2) \qquad (8)$$

for the temperature profiles in RBC proposed by Shishkina & Thess (2009). It can be observed from figures 4 and 5 that the function (8) gives a good approximation of the DNS data, even though the cold boundary layer profile in figure 4 does not follow this approximation. However, figure 8 illustrates that the function (8) gives a reasonable approximation for most temperature profiles when they are normalised with Nu_{loc} as suggested by Ebert *et al.* (2008). The comparison of the diagnostic functions with the results obtained from (8) reveals that the approximation function approaches a value of zero much to rapidly in this case, since the DNS data derease almost linearly for $x_2^+ > 1$.

On the other hand the temperature profiles through the centre of the roll structures show an excellent agreement with the function (8) for both diagnostic functions. We therefore conclude that despite the fact that the plots of θ^+ seem to match for most of the temperature profiles, the diagnostic functions reveal significant differences that reflect a dependency of the profile on the longitudinal position. Therefore the approximation function (8) applies only to temperature profiles with "horizontal" mean flow.

CONCLUSIONS

A comparison of Rayleigh-Bénard convection in a long rectangular enclosure obtained through DNS and detailed experimental measurements of the thermal boundary layers has been conducted. It was shown that the topological structure of the flow field differs when comparing our experimental and numerical data. However, a very good agreement was observed for the temperature profiles through the centre of the roll structures, which is reflected by a good agreement of the diagnostic functions (6) and (7). However, the exponential diagnostic function reveals an offset between DNS and experimental data. It is also observed that both data sets are in better agreement at the higest Rayleigh numbers compared.

Furthermore, we showed that the temperature profiles of the DNS obtained in a closed rectangular cell can (within reasonable accuracy) seem to collapse onto the approximation function proposed by Shishkina and Thess (2009), irrespective of the longitudinal position if the local Nusselt number (thermal boundary layer thickness) is used for the normalisation of the profiles. However, differences between the temperature profiles and the approximation function are observed when the diagnostic functions are evaluated. We therefore conclude that the approximation (8) gives an excellent approximation of temperature profiles if the mean flow is parallel the the heated surfaces.

REFERENCES

Belmonte, A., Tilgner, A. and Libchaber, A., 1994, "Temperature and velocity boundary layers in turbulent convection", *Phys. Rev.*, E 50(1), pp. 269-279.

Chorin, A.J., 1968, "Numerical solution of the Navier-Stokes equations", *Math. Comp.*, Vol. 22, pp. 745-762.

Du Puits, R., Resagk, C., Tilgner, A., Busse, F.H. and Thess, A., 2007, "Structure of thermal boundary layers in turbulent Rayleigh-Bénard convection", *J. Fluid Mech.*, Vol. 572, pp. 231-254.

Ebert, A., Resagk, C. and Thess, A., 2008, "Experimental study of the temperature distribution and local heat flux for turbulent Rayleigh-Bénard convection of air in a long rectangular enclosure", *Int. J. Heat and Mass Tranf.*, Vol. 51, pp. 4238-4248.

Hölling, M. and Herwig, H., 2006, "Asymptitic analysis of heat transfer in turbulent Rayleigh-Bénard convection", *Int. J. Heat and Mass Transf.*, Vol. 49, pp. 1129-1136.

Kaczorowski, M., Shishkin, A., Shishkina, O. and Wagner, C., 2008, "Developement of a Numerical Procedure for direct simulations of turbulent convection in a closed rectangular cell", *New Results in Numerical and Experimental Fluid Mechanics VI*, Vol. 96, pp. 381-388.

Kaczorowski, M. and Wagner, C., 2009, "Analysis of the thermal plumes in turbulent Rayleigh-Bénard convection based on well-resolved numerical simulations", *J. Fluid Mech.*, vol. 618, pp. 89-112.

Maystrenko, A., Resagk, C., and Thess, A., 2007, "Structure of the thermal boundary layer for turbulent Rayleigh-Bénard convection of air in a long rectangular enclosure", *Phys. Rev. E*, Vol. 75(6), 066303.

Schumann, U. Grötzbach, G. and Kleiser, L., 1979, "Direct numerical simulations of turbulence", *Prediction methods for turbulent flows*, VKI-lecture series, Brussels.

Sergent, A. and Le Quéré, P., 2008, Large-scale patterns in a rectangular Raylegh-Bénard cell *Direct and Large Eddy Simulations 7*, Trieste, Italy

Shishkina, O. and Wagner, C., 2007, "Boundary and interior layers in turbulent thermal convection in cylindrical containers", *Int. J. Sci. Comp. Math.*, Vol. 1(2/3/4), pp. 360-373.

Shishkina, O. and Thess, A., 2009, "Mean temperature profiles in turbulent Rayleigh-Bénard convection of water", *J. Fluid Mech.*, submitted.